Supplementary Material (ESI) for Chemical Communications

Synthesis, Characterization and Photophysical Properties of 2-Oxa-bicyclo[3.3.0]octa-4,8-diene-3,6-diones: A New Series of Potential Laser Dyes

Supporting Information

Chao-Yu Wang, Yu-Shan Yeh, Elise Y. Li, Yi-Hong Liu, Shiuh-Ming Peng, Shiuh-Tzung Liu, Pi-Tai Chou**

Department of Chemistry and Instrumentation Center, National Taiwan University, Taipei 106, Taiwan

Experimental

General information Toluene was distilled under N_2 from sodium benzophenone ketyl. Tungsten carbene complex **2** was prepared according to the previously reported method [1]. Chemicals were purchased from commercial sources and used without further purification. Nuclear magnetic resonance spectra were recorded in $CDCl_3$ on either a Bruker AM-300 or AVANCE 400 spectrometer. Chemical shifts are given in parts per million relative to Me_4Si for ^1H and ^{13}C NMR. Infrared spectra were measured on a Nicolet Magna-IR 550 spectrometer (Series-II) as KBr pallets.

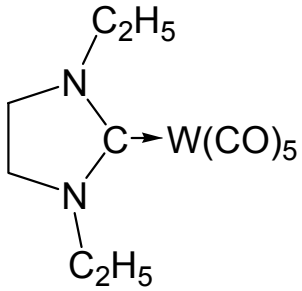

2

Preparation of Compound 1a-1c To an autoclave(100 mL) was loaded with phenylacetylene and rhodium complex (or other metal complexes) in dry toluene. The

reactor was flashed with nitrogen several times. Carbon monoxide was then pressurized and the resulting mixture was stirred at 110°C. After that, solvents were evaporated and the residue was chromatographed on silica gel. The crude product was recrystallized from diethyl ether to give **1a-1c** as red-purple solids.

The NMR and infrared data were reported below.

1a: ^{1}H NMR ($CDCl_3$, 400 MHz): δ 8.54-8.51 (m, 2H), 7.77-7.75 (m, 2H), 7.50-7.39 (m, 6H), 3.69 (s, 2H). ^{13}C NMR ($CDCl_3$, 100 MHz): δ 191.3 (C=O), 170.2 (COO), 150.7, 142.8, 130.9, 130.6, 130.1, 129.9, 128.9, 128.8, 128.6, 128.5, 122.0, 119.1, 44.4 (CH_2). IR (KBr): ($\upsilon_{C=O}$) 1752(s), 1746(s) cm^{-1}.

1b: ^{1}H NMR ($CDCl_3$, 400 MHz): δ 8.54 (d, 2H, *J*=9.2Hz), 7.70 (d, 2H, *J*=9.2Hz), 6.98 (d, 4H, *J*=9.2Hz), 3.87 (s, 6H, *OMe*), 3.64 (s, 2H, C*H*$_2$). ^{13}C NMR ($CDCl_3$, 100MHz): 191.7 (*C*=O), 170.8 (*C*OO), 161.1, 160.6, 140.6, 130.8, 130.2, 123.7, 122.4, 120.4, 117.9, 114.5, 114.0, 55.7 (O*C*H$_3$), 55.6 (O*C*H$_3$), 44.6 (*C*H$_2$). IR (KBr): ($\upsilon_{C=O}$) 1767(s), 1746(s) cm^{-1}.

1c: ^{1}H NMR ($CDCl_3$, 400 MHz): δ 8.50 (d, 2H, *J*=8.8Hz), 7.68 (d, 2H, *J*=8.8Hz), 7.46-7.43 (m, 4H), 3.68 (s, 2H, C*H*$_2$). ^{13}C NMR ($CDCl_3$, 100MHz): 191.4 (*C*=O), 174.8 (*C*OO), 137.5, 136.7, 130.5, 130.0, 129.5, 129.1, 128.2, 127.7, 121.3, 118.5, 44.1(*C*H$_2$). IR (KBr): ($\upsilon_{C=O}$) 1752(s), 1732(s) cm^{-1}.

Crystallography. Crystal suitable for X-ray diffraction analysis was afforded from slow evaporation of the chloroform solution of **1a** at room temperature. Cell parameters were determined either by a Siemens SMART CCD diffractiometer. Crystal data for **1a**: $C_{19}H_{12}O_3$, Fw = 288.29, Orthorhombic, $Pca2_1$, a = 11.7937(4) Å, b = 12.9224(5) Å, c = 18.4121(6) Å, α = 90°, β = 90°, γ = 90°, V = 2806.1(2), Z = 8, $d_{(calcd)}$ = 1.365 Mg/m^3, F(0,0,0) = 1200, 0.20 x 0.15 x 0.10 mm, θ range from 2.21 ° to 25.01°.

2533 reflections with R_{int}=0.1298 out of 12826 total reflections. Full-matrix least-squares on F^2 was used for refinement. R_1=0.0692, wR_2=0.1411 for [$I>2\sigma(I)$]. Tables of atomic coordinates, thermal parameters and bond distances as well as bond angles are deposited in the supporting information. CCDC reference numbers 602233. For crystallographic data in CIF or other electronic format see DOI: 10.1039/b604539a.

Steady state and optical gain measurements Steady-state absorption and emission spectra were recorded with a Hitachi (U-3310) spectrophotometer and an Edinburgh (FS920) fluorimeter, respectively. DCM with an emission yield of ~0.44 (λ_{em} ~ 630 nm) in MeOH served as the standard to calculate the emission quantum yield. Nanosecond lifetime studies were performed with an Edinburgh FL 900 photon-counting system. The emission decays were analyzed by the sum of exponential functions, which allows partial removal of the instrument time broadening and consequently renders a temporal resolution of ~ 200 ps. Optical gain measurements were carried out using the variable stripe length method [2]. In this method, the second harmonic of a *Q*-switched Nd:YAG pumped Ti:Sapphire laser(443nm, pulse width 8ns) was focused into a stripe on the quartz cell by a cylindrical lens. The stripe length was adjusted by a barrier coated with opaque materials. The stripe was aligned near the edge of the square quartz cell, and the emission was collected from the edge at a 90° angle with respect to the excitation beam. The emission was analyzed using a monochromator coupled to a gated ICCD detector.

Theoretical Approach. Time-dependent DFT (TDDFT)[3] calculations using the B3LYP [4] functional were performed based on the structures optimized using the same method with 6-31+G(d) basis. The lowest 10 singlet roots of the nonhermitian eigenvalue equations were obtained to determine the vertical excitation energies. Oscillator strengths were deduced from the dipole transition matrix elements. The

excited-state TDDFT calculations were carried out using Gaussian03 as described in our previous publications [5].

Table S1. Selected bond distances(Å), bond angles(deg) and dihedral angles(deg) of **1a**.[a] See Figure S7 for the numerical assignment.

C(1)-C(2)	1.49(1)	C(2)-C(3)	1.370(9)
C(3)-C(4)	1.485(9)	C(4)-C(5)	1.515(9)
C(5)-C(6)	1.537(8)	C(6)-C(7)	1.348(9)
C(7)-O(1)	1.385(8)	O(1)-C(1)	1.400(8)
C(6)-C(8)	1.45(1)	C(2)-C(14)	1.46(1)
C(20)-C(21)	1.484(9)	C(21)-C(22)	1.36(1)
C(22)-C(23)	1.483(9)	C(23)-C(24)	1.498(9)
C(24)-C(25)	1.514(8)	C(25)-C(26)	1.333(9)
C(26)-O(4)	1.376(7)	O(4)-C(20)	1.407(8)
C(25)-C(27)	1.45(1)	C(21)-C(33)	1.46(1)
O(1)-C(1)-O(2)	118.3(6)	O(2)-C(1)-C(2)	132.2(6)
C(1)-C(2)-C(14)	123.8(6)	C(2)-C(3)-C(4)	144.0(7)
C(3)-C(4)-O(3)	128.8(7)	C(4)-C(5)-C(6)	106.1(5)
C(5)-C(6)-C(8)	123.9(5)	C(6)-C(7)-O(1)	131.7(6)
O(4)-C(20)-O(5)	119.1(6)	O(5)-C(20)-C(21)	131.8(6)
C(20)-C(21)-C(33)	123.8(6)	C(21)-C(22)-C(23)	145.0(7)
C(22)-C(23)-O(6)	128.0(7)	C(23)-C(24)-C(25)	105.3(5)
C(24)-C(25)-C(27)	123.4(5)	C(25)-C(26)-O(4)	133.7(7)
C(6)-C(7)-C(3)-C(2)	-179.5(6)	C(4)-C(3)-C(7)-O(1)	179.7(5)
C(3)-C(2)-C(14)-C(15)	- 4(1)	C(7)-C(6)-C(8)-C(9)	2(1)
C(14)-C(2)-C(1)-O(2)	- 2(1)	O(3)-C(4)-C(3)-C(2)	- 3(1)
C(25)-C(26)-C(22)-C(21)	179.3(6)	C(23)-C(22)-C(26)-O(4)	179.0(6)
C(22)-C(21)-C(33)-C(34)	169.4(7)	C(26)-C(25)-C(27)-C(28)	176.1(6)
C(33)-C(21)-C(20)-O(5)	-1(1)	O(6)-C(23)-C(22)-C(21)	3(1)

[a] This system is statistically in between centrosymmetric and non-centrosymmetric space group. The structure was solved under the non-centrosymmetric space group. Alternatively, we have made an attempt to solve the structure by using a centrosymmetric space group but unfortunately failed.

Table S2. The calculated energy levels of the lower-lying transitions of **1a.**

	Assignments	[nm]	E [eV]	*F*
S_1	HOMO→ LUMO(+72%)	472.6	2.62	0.7233
S_2	HOMO-4 → LUMO(+92%)	405.6	3.06	~0
S_3	HOMO-1 → LUMO(+95%)	388.6	3.19	0.0076
S_4	HOMO-2 → LUMO(+82%)	353.3	3.51	0.0304
S_5	HOMO-3 → LUMO(+92%)	348.9	3.55	0.0020

Table S3. The calculated energy levels of the lower-lying transitions of **1b.**

	Assignments	[nm]	E [eV]	*F*
S_1	HOMO→ LUMO(+72%)	513.3	2.42	0.9109
S_2	HOMO-3 → LUMO(+92%)	396.4	3.13	~0
S_3	HOMO-1 → LUMO(+84%)	390.4	3.18	0.0111
S_4	HOMO-2 → LUMO(+95%)	358.5	3.46	0.0002
S_5	HOMO-4 → LUMO(+88%) HOMO → LUMO+2(5%)	328.4	3.78	~0

Table S3. The calculated energy levels of the lower-lying transitions of **1c.**

	Assignments	[nm]	E [eV]	*F*
S_1	HOMO→ LUMO(+73%)	488.8	2.54	0.8903
S_2	HOMO-3 → LUMO(+92%)	406.4	3.05	~0
S_3	HOMO-1 → LUMO(+84%)	373.7	3.32	0.0117
S_4	HOMO-2 → LUMO(+93%)	368.1	3.37	0.0093
S_5	HOMO-4 → LUMO(+93%)	334.1	3.71	0.0037

Figure S1. ^{1}H-NMR spectra of **1a**.

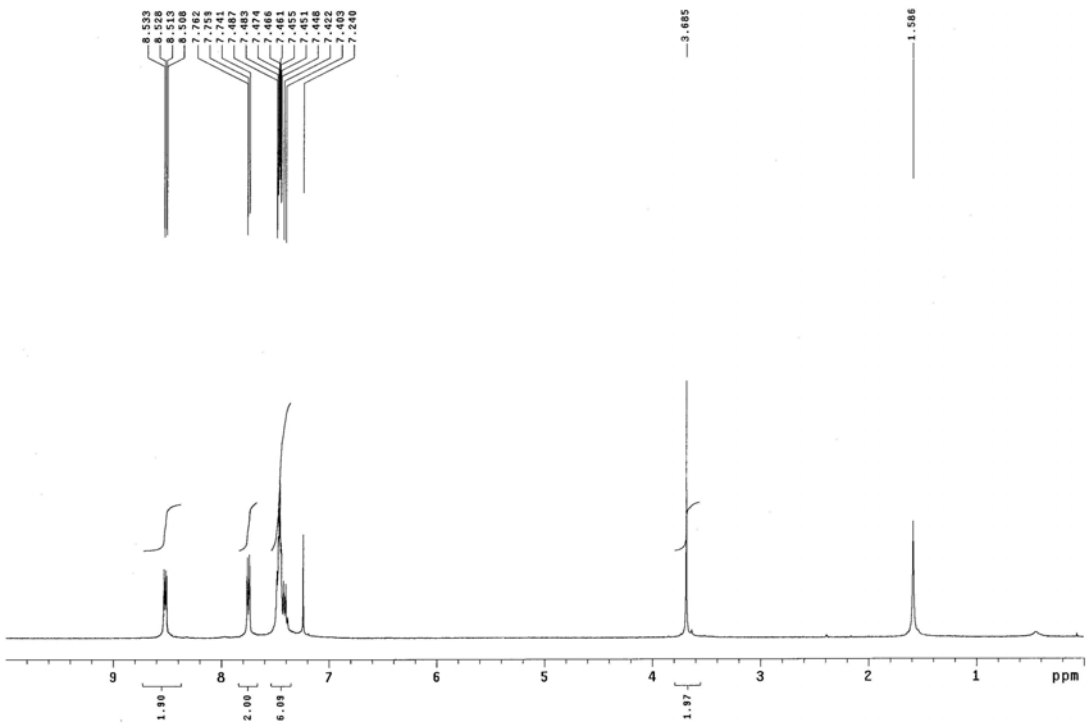

Figure S2. ^{1}H-NMR spectra of **1b**.

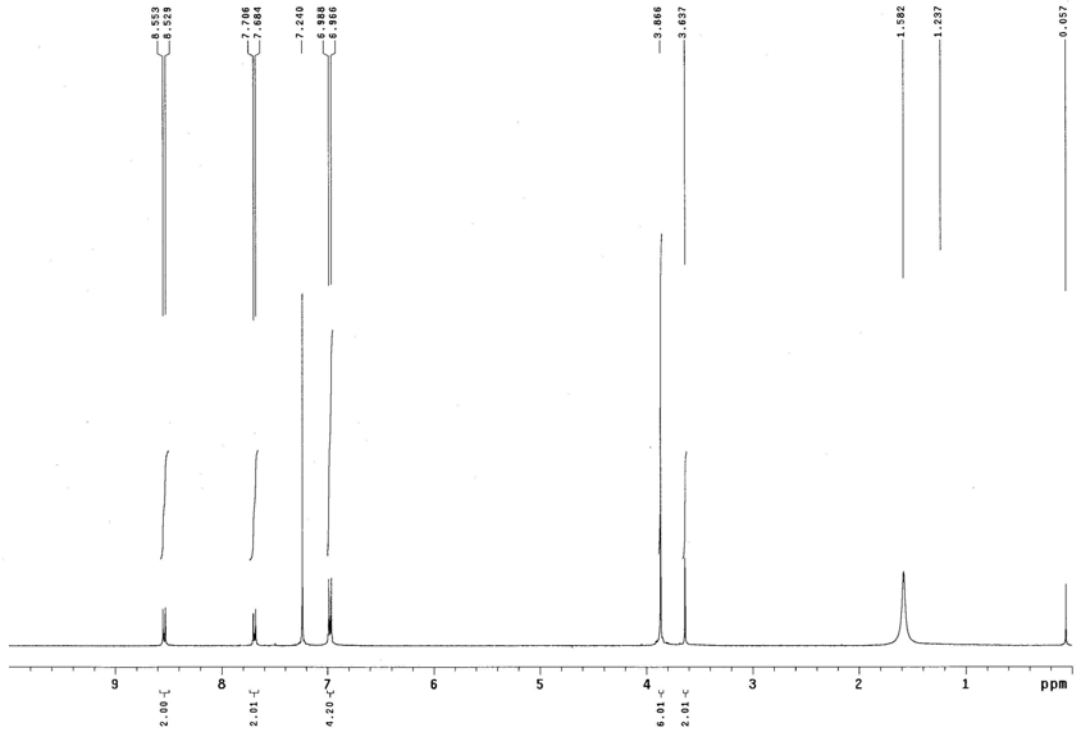

Figure S3. ^{1}H-NMR spectra of **1c**.

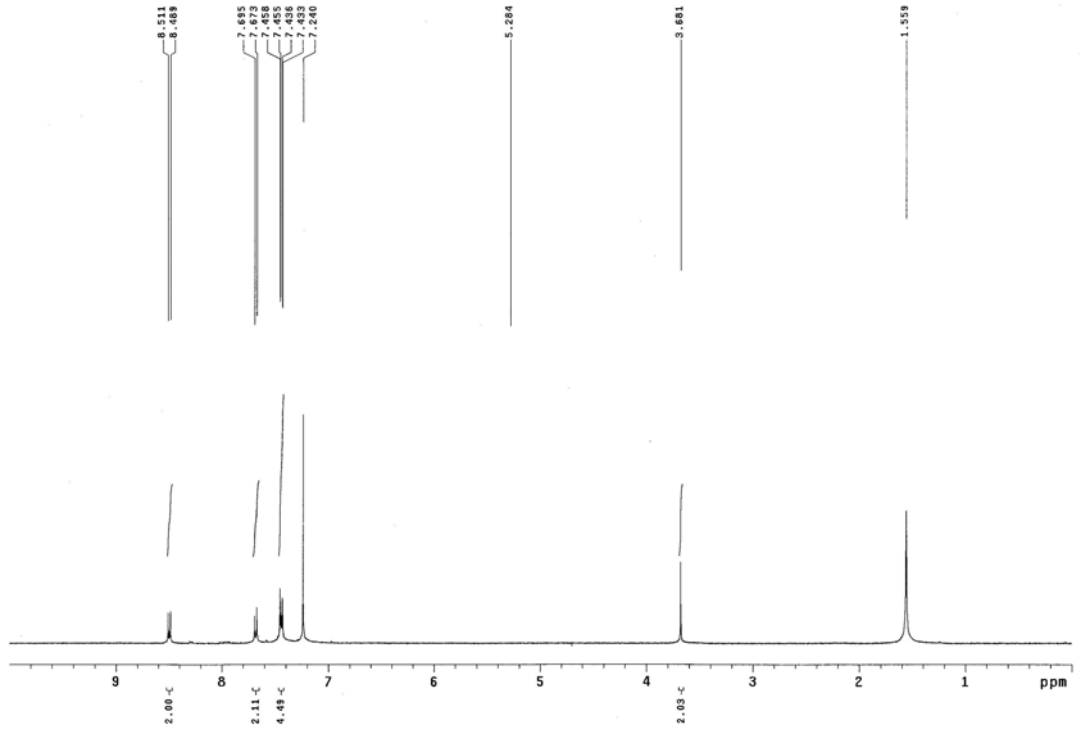

Figure S4. Selected frontier orbitals of **1a** involved in the lower lying transitions.

HOMO	LUMO
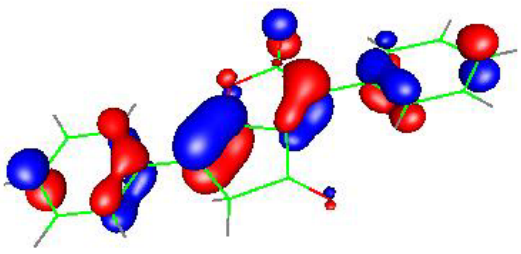	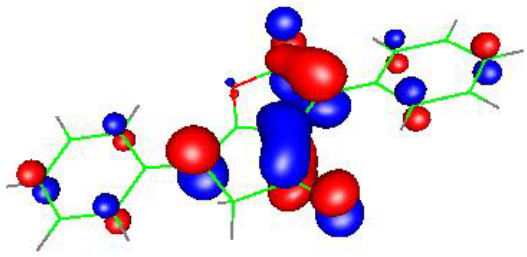
HOMO-2	HOMO-1
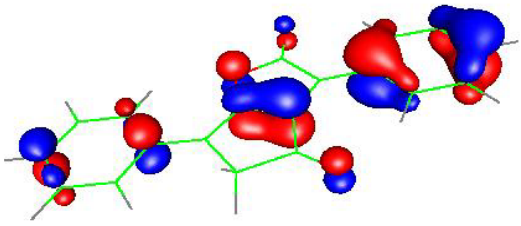	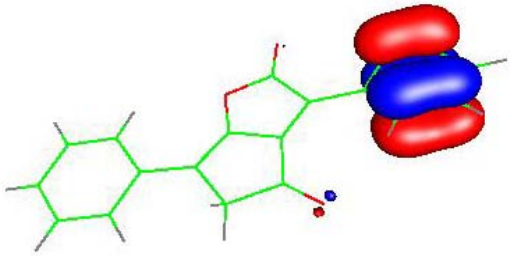

HOMO-4	HOMO-3
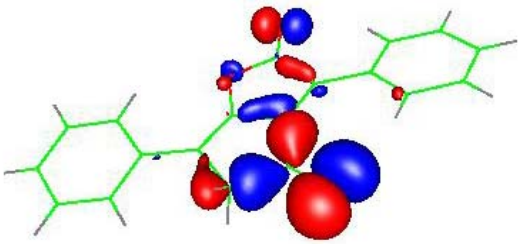	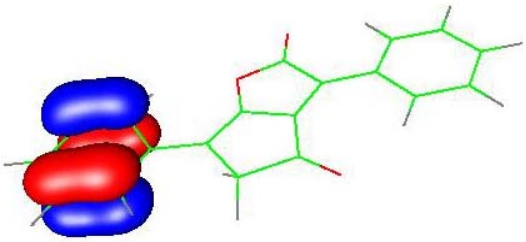

Figure S5. Selected frontier orbitals of **1b** involved in the lower lying transitions.

HOMO	LUMO
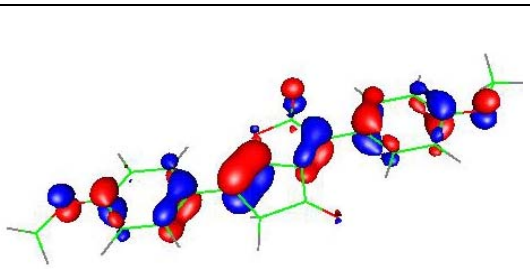	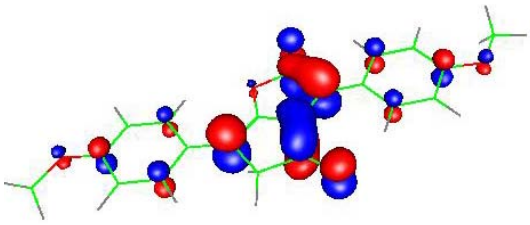
HOMO-2	HOMO-1
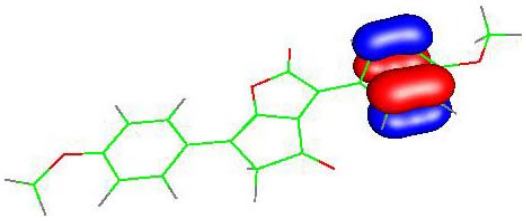	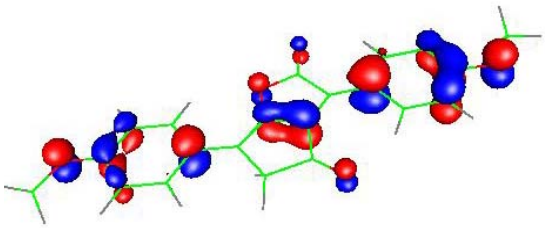
HOMO-4	HOMO-3
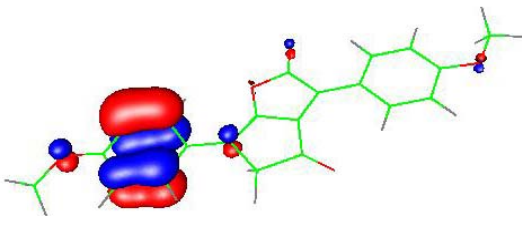	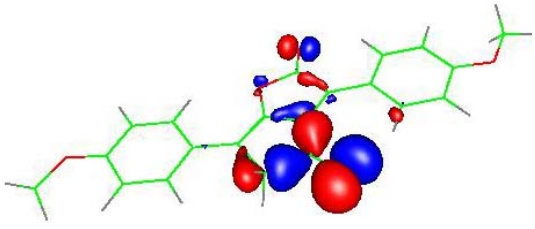

LOMU+1	
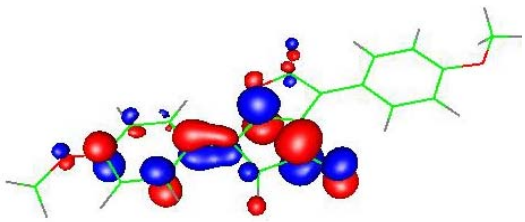	

Figure S6. Selected frontier orbitals of **1c** involved in the lower lying transitions.

HOMO	LUMO
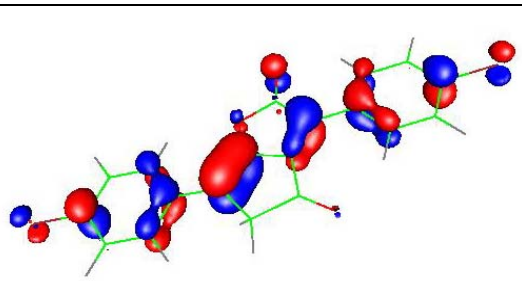	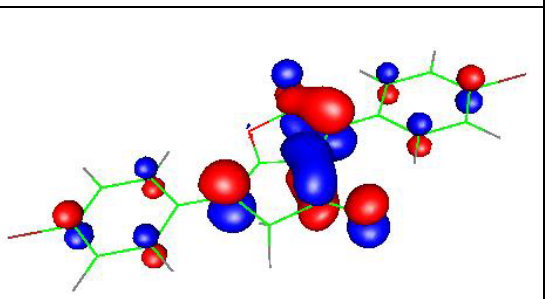
HOMO-2	HOMO-1
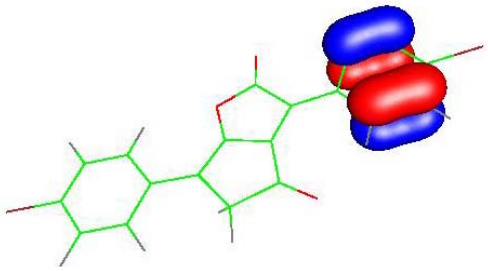	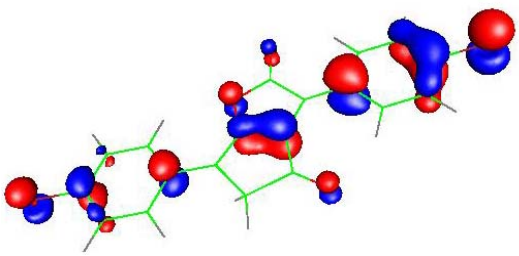
HOMO-4	HOMO-3
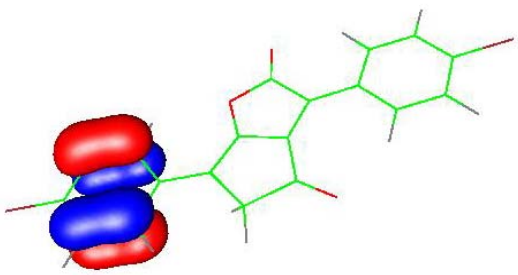	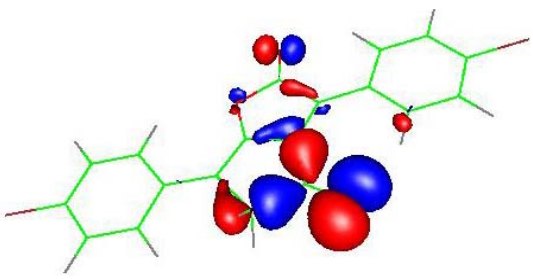

Figure S7. ORTEP Plot of **1a** (including two independent molecules) with ellipsoids drawn at the 30% probability level.

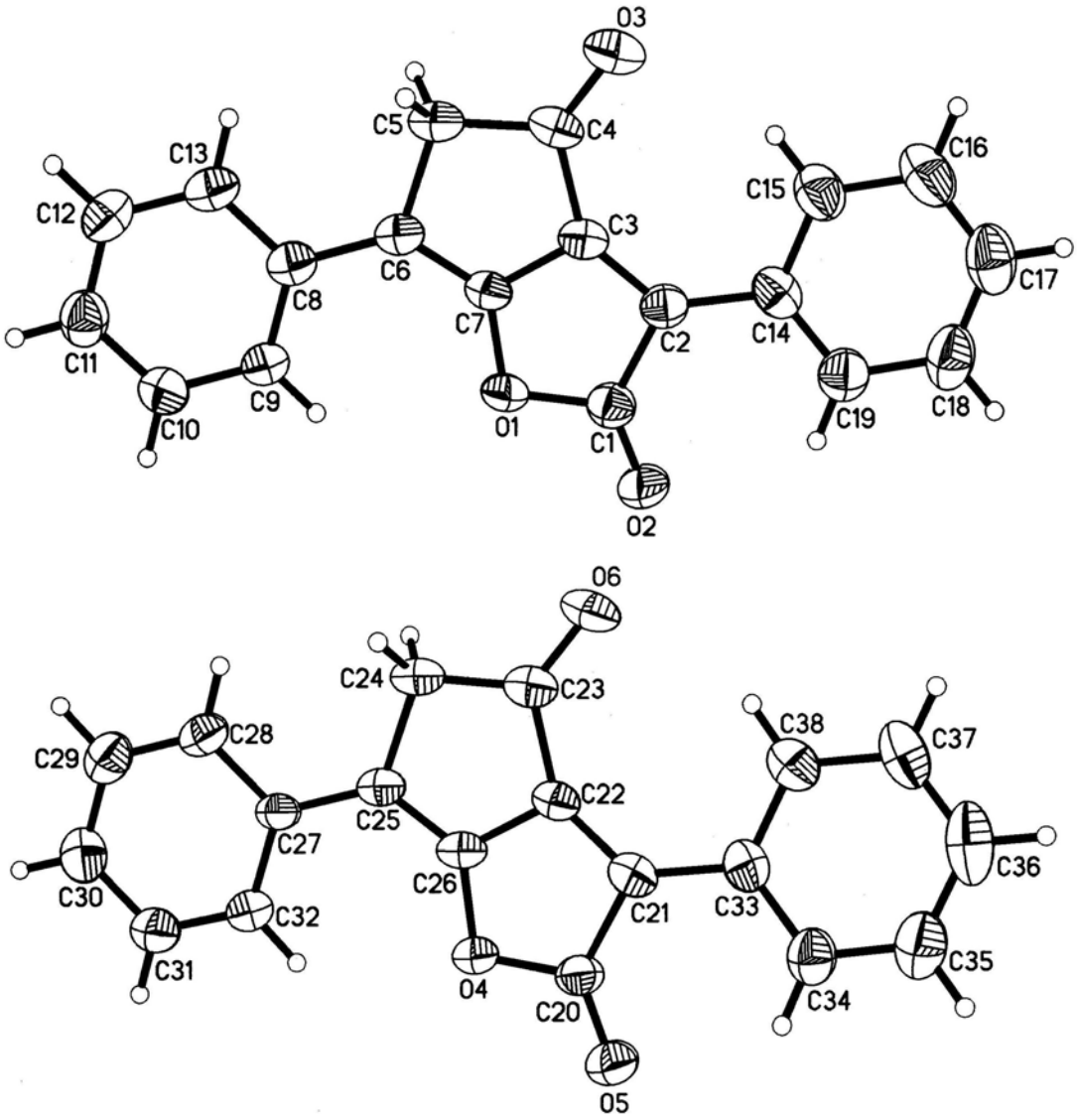

References:

1. C.-Y. Liu, D.-Y. Chen, G.-H. Lee, S.-M. Peng and S.-T. Liu *Organometallics,* 1996, **15,** 1055.

2. K. L. Shaklee, R. E. Nahory and R. F. Leheny, *J. Lumin*., 1973, **7**, 284.

3. (a) C. Jamorski, M. E. Casida and D. R. Salahub, *J. Chem. Phys.,* 1996, **104**, 5134. (b) M. Petersilka, U. J. Grossmann and E. K. U. Gross, *Phys. Rev. Lett.,* 1996, **76**, 1212. (c) R. Bauernschmitt, R. Ahlrichs, F. H. Hennrich and M. M. Kappes, *J. Am. Chem. Soc.,* 1998, **120**, 5052. (d) M. E. Casida, *J. Chem. Phys.,* 1998, **108**, 4439. (e) R. E. Stratmann, G. E. Scuseria and M. J. Frisch, *J. Chem. Phys*., 1998, **109**, 8218.

4. (a) C. Lee, W. Yang and R. G. Parr, *Phys. Rev. B,* 1988**, 37**, 785. (b) A. D. Becke, *J. Chem. Phys.,* 1993, **98**, 5648.

5. J.-K. Yu, Y.-M. Cheng, Y.-H. Hu, P.-T. Chou, Y.-L. Chen, S.-W. Lee, Y. Chi, *J. Phys. Chem. B,* 2004, **108**, 19908.